Experimental Investigation of Zinc Antimonide Thin Film Thermoelectric Element over Wide Range of Operating Conditions

Hosseini, Seyed Mojtaba Mir; Rezaniakolaei, Alireza; Blichfeld, Anders Bank; Iversen, Bo Brummerstedt; Rosendahl, Lasse Aistrup

Experimental Investigation of Zinc Antimonide Thin Film Thermoelectric Element over Wide Range of Operating Conditions

M. Mirhosseini[1], A. Rezania[1,*], A. B. Blichfeld[2,3], L. A. Rosendahl[1]

[1] Department of Energy Technology, Aalborg University, Pontoppidanstraede 111, 9220 Aalborg East, Denmark

[2] Centre for Materials Crystallography, Department of Chemistry and iNANO, Aarhus University, Langelandsgade 140, DK-8000 Aarhus C, Denmark

[3] Current address: Department of Materials and Engineering, Norwegian University of Science and Technology (NTNU), NO-7491, Trondheim, Norway.

Abstract

Zinc antimonide compound is one of the most efficient thermoelectric (TE) materials known at moderate temperatures up to 350 °C for its exceptional low thermal conductivity. This study aims to evaluate performance of a thin film TE deposited on an insulating substrate, while the heat flows laterally in the thin film. At first, effect of applying different temperatures at hot side of the specimen is investigated to reach steady state in open circuit analysis. Then, the study focuses on performance and stability analysis of the thermoelectric element operating under different load resistances and over wide range of operating temperatures from 160 °C to 350 °C. The results show that, at hot side temperature equal to 275 °C, the Seebeck coefficient (α) reaches its maximum value (242 µV/K), which is comparable to that of bulk materials reported in the literature. According to variation of the load resistance, the maximum output power, that is a function of temperature, occurs at 170.25 Ω. The maximum power is 8.46 µW corresponding to a cold and hot side temperature of $\approx$ 30 °C and 350 °C, respectively.

Keywords*: Thin Film TEG; Maximum Output Power; Seebeck Coefficient; Zinc Antimonide; Load Resistance.*

1. Introduction

Thermoelectric (TE) devices have been employed for many years as a reliable energy conversion technology for applications ranging from the cooling devices to the direct conversion of heat into electricity for power generation.

---

[*] Corresponding author: Alireza Rezaniakolaei. E-mail: alr@et.aau.dk

26   The efficiency of TE materials is evaluated using the dimensionless figure of merit, $zT = \alpha^2 T /(\rho \kappa)$, where α is the

27   Seebeck coefficient, T is absolute temperature, ρ is electrical resistivity and κ is the total thermal conductivity consisting

28   of contribution from the charge carrier κ_e and the lattice κ_L. TE materials with $zT > 1$ can typically give a reasonable

29   efficiency (e.g. 5%), but in fact for commercial applications it is equally important that the TE materials are made of

30   cheap and abundant elements with cost-effective synthesis methods [1].

31   Although most research concerns bulk materials for high power applications such as recovery of waste heat from car

32   exhaust, attractive low power applications of thin films are evident. The inherent phonon scattering due to the

33   nanostructure of thin films can be exploited to enhance TE properties [2]. As a new kind of environmentally friendly

34   material, ZnSb is made of relatively cheap and nontoxic elements.

35   The Zn–Sb binary system contains ZnSb and β-Zn_4Sb_3 which are promising p-type thermoelectric materials for low cost

36   thermoelectric application, intended to operate at intermediate temperatures (from room temperature to 350 $^\circ$C) [3].

37   Thin film technique is a promising method for improving the thermoelectric properties of thermoelectric material due to

38   low dimensional quantum confinement and a much lower lattice thermal conductivity [4]. Properties of the thin film

39   thermoelectric materials have introduced a huge potential in application of miniaturization sensors, micro-power source

40   and other thermoelectric applications of the thin film thermoelectric devices. Moreover, for many micro scale TE

41   devices, thin films are highly required [5]. Therefore, thin films can offer tremendous scope for enhancement the figure

42   of merit. There are some researches for basic evaluation of TEG devices or samples under different conditions, where

43   very few of them are based on zinc antimonide TE material. The efficiency of a commercial TEG under thermal cycling

44   was investigated by Hatzikraniotis *et al.* [6]. They investigated long time performance and stability of a commercially

45   available TEG under variable temperature and load cycling. The module was subjected to sequential hot side heating (at

46   200 °C) and cooling for long times (3000 h) in order to measure changes in the TEG's performance. A reduction of

47   3.8% in Seebeck coefficient, a 16.1% increase in resistivity and 6.6% decrease in the average leg thermal conductivity

48   were observed. In a study by Sun *et al.* [7], zinc antimonide films were deposited on polished fused silica substrates by

49   co-sputtering of a Zn target and a specifically prepared Zn-Sb compound target. The TE measurements were subjected

50   to two measurement cycles, *i.e.* room temperature $(RT) \rightarrow 573$ K $\rightarrow RT \rightarrow 573$ K $\rightarrow RT$. It was seen that the TE

51   properties of the film become stable after the first heating cycle. The stable power factor (PF) of their Zn_4Sb_3 film

52   during the two measurement cycles implied a good phase stability of Zn_4Sb_3 at $T \leq 573$ K in a low pressure inert

53   atmosphere.

Yan and Malen [8] showed that the use of a periodic heat source, instead of a constant heat source, can improve the conversion efficiency of a thermoelectric power generator. In addition, they presented experimental measurements on a commercial thermoelectric device (bismuth telluride based device) to validate analytical and numerical models. These models showed that maximum efficiency is achieved when the period of the heat source is much larger than the thermal time constant of the thermoelectric power generator.

In a study on zinc antimonide compounds [3], it was found that the thermoelectric properties of Zn-Sb thin films are sensitively related to the phase transformation. The deposited thin films were annealed at 673 K under Ar atmosphere for 1 hr. X-ray diffraction (XRD) results showed that the thin film gradually transforms from β phase Zn_4Sb_3 to ZnSb phase with increasing Sb sputtering power. Moreover, an enhanced power factor of 1.91×10^{-3} W/m K^2 was obtained through optimizing the ratio of β-Zn_4Sb_3 to Zn-Sb phase in the mixed Zn-Sb thin film. For all the specimens, Seebeck coefficient increased by temperature from 300 to 573 K.

Zinc antimonide thin film specimens were deposited on polyimide substrate by radio frequency sputtering method at room temperature [9]. All the specimens were annealed in argon atmosphere at different temperatures and the thermoelectric properties of all the thermoelectric elements were significantly boosted. The power factor of thin films annealed at 325 °C was higher than other specimens. After improving properties, the specimens were tested in different working temperatures from 50 to 260 °C. The maximum Seebeck coefficient of 280 µV K^{-1} and the maximum power factor of 2.35×10^{-3} Wm^{-1} K^{-2} was obtained at 260 °C.

Fan et al. [10] demonstrated a promising flexible thin film thermoelectric generator using the n-type Al-doped ZnO and p-type Zn-Sb based thin film. Their flexible substrate was suitable to be used under 520 K. They showed that the output power of their generator is 4 times higher than those in the literature, while it is 4-5 times cheaper.

Brinks et al. [11] investigated on thermal stability enhancement of thermoelectric $Ca_3Co_4O_9$ thin films up to 550 °C in an oxygen rich environment. The thermal stability and high temperature thermoelectric properties were studied by electrical resistivity and Seebeck measurements by thermal cycling. In contrast to generally performed heating in helium gas, it was shown that an oxygen/helium mixture provides sufficient thermal contact, while preventing the previously disregarded formation of oxygen vacancies. The resistivity is much more sensitive to the background gas during thermal cycling than the Seebeck coefficient in thin film and bulk $Ca_3Co_4O_9$.

In another study on thin film TEGs, Daniel et al. [12] studied thermal stability of thermoelectric $CoSb_3$ skutterudite thin films. It was shown that an excess of Sb stabilizes the $CoSb_3$ skutterudite phase. Furthermore, resistivity was stable during thermal cycling as long as the temperature was kept below the initial annealing temperature.

83   Shim *et al.* [13] discovered that, as the number of thermal cycle increases, the power factor of Zn_xSb_y thin films is

84   reduced. This degradation is more pronounced in an inert gas atmosphere than in ambient surroundings. The main

85   reason of this degradation was closely related to the reduction in the electrical conductivity of the Zn_xSb_y thin film,

86   which is associated with thermal decomposition. Fan et al. [14] demonstrated the properties of their designed thin film

87   thermoelectric generators with heat flow running in longitudinal direction of the film, where the maximum temperature

88   difference between both sides is maintained 85 ℃. N-type Bi_2Te_3 and p-type Sb_2Te_3 thin films were deposited on soda-

89   lime glass substrates. They argued that the performance of thin film TEG with this structure can be further improved by

90   optimizing thermoelectric materials and fabrication methods. In a conventional thin film TEG as reported in most of the

91   above references, heat flow running perpendicular to the film surface is widely used. In these thin films, the hot side and

92   cold side are just separated by the thickness of the films. The temperature of the cold side increases immediately by the

93   heat transferred from the hot side, and the temperature difference between both sides will be alleviated greatly in a very

94   short time. Due to the small temperature difference, conventional thin films usually have low output power even though

95   the figure of merit of the materials used for thin films is high. This kind of TE modules needs an efficient cooling

96   technology with high cooling energy to keep the cold side temperature low that is not efficient from aspect of net

97   energy and economy. Accordingly, to produce more electrical potential difference by using thin film based

98   thermoelectric module, one way is that heat flow runs lateral to the surface of thin films deposited on an insulating

99   substrate. One advantage of using the thermoelectric element laterally is that, due to high thermal resistance of the

100   thermoelectric element, there is no need for an efficient heat sink in order to provide an efficient TE module.

101   There are only references [10, 14] which discuss only about the thermoelectric properties of a thin film p-n couple and

102   modules in steady state which heat conducts in the longitudinal direction parallel to thin film surface by using constant

103   hot side temperatures when the cold side is exposed to the environmental temperature. Therefore, present study

104   investigates the performance of a zinc antimonide specimen as a p-type leg of a TE module under transient as well as

105   steady state thermal boundary condition close to practical conditions.

106

107   **2.   Experimental apparatus and procedures**

108   **2.1. Thin film production**

109   The thin films are produced by magnetron co-sputtering deposition at Aarhus University, Denmark. The Zn-Sb film was

110   directly deposited on fused silica substrates. One target was a commercial Zn-target, whereas the other was produced in-

4

house by the process reported by Yin *et al.* [15]. The substrate is a 180 μm thick single-sided polished fused silica wafer. The substrate was heated to 215 °C during the deposition, to allow for crystallization of the film. Argon (purity 99.9996%) was used as sputter gas at a flow rate of 10 sccm and the Ar pressure in the chamber was fixed at 0.6 Pa with a deposition time of 60 minutes. The power for the Zn_4Sb_3 and Zn targets were fixed to 12 W and 4 W, respectively. The chamber base pressure was approximately 3×10^{-5} *P*a. The phase transitions of the film were confirmed directly by in situ powder X-ray diffraction (PXRD) and further evidenced through the changes in the electrical properties. The as-deposited and annealed specimen was characterized by SEM (Nova600 NanoLab, FEI) with EDX, PXRD (D8 Discover, Bruker AXS) in θ –2θ geometry with CuKα radiation, and in situ PXRD. The film thickness is about 600 nm, which was measured from the cross sectional SEM image. Before and after the annealing treatment, no change of the film thickness was observed.

This thermoelectric element has been produced with atomic ratio (Zn:Sb) as mentioned in Table 1. This is roughly the same as for the Zn-Sb film reported by Sun et al. [7]. XRD pattern is shown in Fig. 1 for the specimen.

The ratio of ZnSb: Zn_4Sb_3 is ~ 6:4, so ZnSb is the dominant phase. The photograph of this specimen before the tests is also shown in Fig. 1. The specimen is a rectangular thin film by the length and width equal to 19.8 and 17.2 mm, respectively. The length of hot side and cold side contact area is equal to 3 mm that should be subtracted from the total length to obtaining the effective length.

2.2. Thin film test bench

The test device integrated on the bench (Fig. 2) with ability of heating the hot side up to 400 °C. This device is for testing any kind of coated TE thin film thermoelectric elements and TE single legs. There is integrated separately cooling system of the cold side, but in the present study by assuming environmental temperature for the cold side of the specimen, this part of the test bench is not used. Thus, the cold side of the specimen is only in contact with cold side block without any forced convection cooling during the test. The temperature of the hot side can be adjusted between 150 °C and 400 °C. The hot and cold side temperatures are measured by probes mounted on both sides of the specimen. In the present study, a wide range of temperatures at the hot side and room temperature at the cold side of the specimen are applied in order to measure performance of the thin film element. Nine temperatures at hot side of the specimen are provided; 160, 175, 200, 225, 250, 275, 300, 325, and 350 °C. After some minutes from the beginning of each test, the

139 specimen operates under steady state condition. Whole measurement time by data logger is 4500 seconds for each

140 experiment. Data sampling rate was 0.25 Hz, giving 300 data points for each test.

141

142 **3. Results and discussion**

143 **3.1. Open circuit analysis**

144

145 Fig. 3 shows the hot side temperature of the specimen during the time. According to the figure, the condition can be

146 assumed steady state after a short transient region. In Fig.4, voltages versus time are observed. Voltage in open circuit

147 condition has similar trend with the hot side temperature with respect to time.

148 Variation of the voltage versus temperature difference ($\Delta T = T_{hot} - T_{cold}$) is shown for different hot side temperatures in

149 Fig.5. The trend of the figure is approximately linear for all cases, showing that the voltage is increasing by raising the

150 temperature difference for all cases almost with the same slope. According to different hot side conditions, passing from

151 unsteady area is not exactly the same even in the same temperature difference. It is due to several parameters such as

152 thermal diffusivity which can change by temperature. In other words, in the transient area, there is not exactly a single

153 voltage data point for each temperature difference since different boundary conditions are applied. In each data set, the

154 voltage data points in transient condition are dispersed, while the data points related to the steady state condition are

155 obviously aggregated. When the system is thermally balanced and reached the steady state condition, almost 280 data

156 points are collected which are much closer together unlike the transient conditions.

157 Moreover, in sub-Fig.5, the voltage versus hot side temperatures is shown for steady state condition. The figure has

158 been obtained by end values of voltage at colored marker data sets in Fig. 5. It seems a linear approximation will also be

159 a convenient fitting for the sub-Fig. 5.

160 The Seebeck coefficient (α) versus the hot side temperature is shown in Fig.6. Using the hot and cold side temperatures

161 and the voltage to calculate instantaneous Seebeck coefficient shows interesting trend of this coefficient until the steady

162 state condition is reached. Nevertheless, definition of the Seebeck coefficient could be applicable also in transient

163 conditions; under such conditions where it can be named as transient Seebeck coefficient.

164 When the accumulation of the data points related to the maximum hot side temperature increases to its extreme, it

165 means the system reaches steady state condition; where the final value of these Seebeck coefficients occurs.

166   The obtained value of α for this specimen is in agreement with new developed TEG materials and zinc antimonide

167   compounds in literature [7, 9-11, 13, 16].

168   The values of Seebeck coefficient with respect to time are shown in Fig. 7. It is worthy to mention that the Seebeck

169   coefficient is a material's property. The first data point in each data set is related to data recorded at the moment the

170   heater is turned on. In other words, the first calculated value of Seebeck coefficient is equal to the Seebeck coefficient

171   in ambient temperature. Ignoring the first data point, the rate of increasing the temperature difference between the

172   specimen's junctions is lower than increasing the voltage in a short range of transient area. That is due to higher thermal

173   conductivity of ZnSb at lower temperature ranges, whereas it decreases by increasing the temperature [7, 13]. In

174   continue, in the rest of the transient area, the rate of increasing the temperature difference is higher than increasing the

175   voltage and the value of transient Seebeck coefficient is alleviated to reach its own steady state values. In steady area,

176   these values are very close to each other during the tests in spite of different thermal conditions.

177   With a detailed evaluation of the Seebeck coefficients in steady state in Fig.8, this coefficient varies with different

178   thermal conditions. This figure is a criterion for clear comparison of Seebeck coefficients versus the hot side or average

179   temperature of the specimen. The Seebeck coefficient is observed to increase up to a maximum (242 µV/K) and then

180   decreases. Although, its variation is negligible especially for operating temperature of hot side between 275 °C and 350

181   °C, but the maximum point is interesting. Herein, the contribution of the third factor of thermal conductivity to the total

182   thermal conductivity is appeared, namely bipolar transport. When the hot side temperature increases more than 275 °C,

183   the bipolar transport effect arises because of the two types of charge carriers, namely electrons and holes. The bipolar

184   transport increases due to the excitation of electrons from the valence band to the conduction band as the temperature is

185   increased, creating an equal number of holes. These holes and electrons will then move to the cold side and transport

186   heat from the hot side to the cold side of the specimen. However, the net electrical current is zero in this movement due

187   to the equal numbers of opposite charges, but finally, the presence of both electrons and holes will have a negative

188   effect on the Seebeck coefficient. Therefore, bipolar effect happens whenever the temperature of the whole

189   thermoelectric element or even a part (section) of it is more than an individual temperature which related to the type of

190   material, its manufacturing process and impurities in its structure, etc. In other words, bipolar affects the whole body of

191   the TE specimen or device and its characteristics such as total Seebeck coefficient, electrical resistivity, and thermal

192   conductivity, even if it happens only near the hot side.

193   The trend of Seebeck coefficient by increasing the temperature is similar to the results in reference [16] for zinc

194   antimonide specimen without doping by silver (Ag). In sub-Fig. 8, Seebeck coefficient is shown for a thin film that has

7

been previously produced by the same procedure and composition [7]. It can be observed that the bipolar transport happens near the temperature 263 °C, whereas in our study, it happens in hot side temperature 275 °C. Thus, bipolar transport happens almost in the same temperature. Certainly, this device and procedure for testing the thin film specimen is different with the device and method that they used in their study [7]. Figure 9 shows the electrical resistivity of the specimen versus time. In Fig. 10, the electrical resistivity and thermal conductivity of the thermoelectric element are represented for various average temperatures in steady state condition. Both data series in the figure reduce slightly by raising the hot site temperature. By using the relation 1 and 2 for calculating the figure of merit (ZT) and efficiency (η), Fig. 11 is drawn. In these calculations, the Seebeck coefficient that was shown in Fig. 8, and thermal conductivity and electrical resistivity from Fig. 10 are used.

$$ZT = \frac{\alpha^2 T}{\rho \kappa} \tag{1}$$

$$\eta = \frac{T_h - T_c}{T_h} \frac{\sqrt{1+ZT}-1}{\sqrt{1+ZT}+\frac{T_c}{T_h}} \tag{2}$$

where α is the Seebeck coefficient [V/K], T [K] is the mean temperature of the thermoelectric element, ρ [Ω.m] is the electrical resistivity, κ [W/m.k] is the thermal conductivity, T_h and T_c are hot and cold side temperature, respectively.

As seen in Fig. 11, by increasing the hot side temperature, both figure of merit and efficiency increase. The maximum efficiency of the specimen in this operating condition is about 7.4%. The hump on the figure of merit curve (at hot side temperature 275 °C) is directly related to Seebeck coefficient values trend (Fig. 8) as seen in equation 1. But, the hump is not clearly disclosed in the curve of efficiency. The results in Figs. 10 and 11 are brought versus average temperature to be comparable with the results of reference [7] in the mentioned temperature range.

3.2. Close circuit analysis

In this part, the study focuses on stability analyzing of power generation by the specimen operating under different load resistances at above mentioned thermal conditions in steady state.

A wide range of load resistance (from 10 to 300 Ω) is applied with a 10 Ω step to find optimal electrical load value giving the maximum power generated by the specimen. It must be mentioned that at first the specimen thermally reaches steady state condition without load, and then the load is applied. Whenever the under loaded thermoelectric element reaches steady state condition, as electronically at each temperature, the next higher load is applied. The time

221 interval for each load value is chosen 5 minutes to ensure the thermoelectric element reaches steady state condition

222 under the applied electrical load.

223 Based on theory, maximum power is produced when the value of the external load is equal to the thermoelectric

224 element resistance. In the present study, due to unavoidable contact resistance, the maximum output power happens

225 when the external load is equal to the thermoelectric element resistance plus contact resistance. Internal resistance of the

226 thermoelectric element plus contact resistance in environment temperature is equal to 188.3 Ω. By having the electrical

227 resistivity (from Fig. 10) and the geometry of the thermoelectric element, internal resistance of it can be calculated by

228 relation 3.

229

230
$$R = \frac{\rho L}{A}$$
(3)

231 where L and A are the effective length and cross section area of the specimen, respectively.

232 Due to restriction for bracing the thermoelectric element (comprised thin glass substrate) in joint locations, the amount

233 of contact resistance in a real application inevitably is several times more than the internal resistance of the specimen.

234 The thermoelectric element electrical resistance will have a huge difference to that one including contact resistance

235 shown in Fig. 12; but the value of both of them is slightly decreasing by raising the temperature. Testing the specimen

236 by different loads shows that peak power is produced in a load resistance very close to the slope of V-I linear

237 distribution, separately for each thermal condition. Also, for all curves in Fig. 13, power increases to a maximum value,

238 and decreases afterwards. The maximum power occurs at external loads 170-190 Ω. The peak power is 8.46 μW

239 corresponding to the hot side temperature 350 °C and external load equal to 170.25 Ω; whereas the peak power by the

240 specimen without considering contact resistance effect can be calculated by relation 4 and is 127.21 μW (Fig. 14).

241
$$P = \frac{\alpha^2 (\Delta T)^2}{\rho} \frac{A}{L}$$
(4)

242

243 The percentage of difference between two series of results in Fig. 14 is about 93-94%, that shows the improvement of

244 electrical conductivity at contact locations can reduce the waste power seriously. At the end of tests, further open

245 circuit tests are taken to check degradation of the Seebeck coefficient to ensure stability of the thermoelectric element

246 during the tests.

247

248 **4.   Conclusions**

249   An efficient thin film TEG module based on p-n couples can be designed and fabricated since a fundamental

250   investigation is firstly done to analyze the performance of the uni-thin film specimen. Present study investigated

251   performance of a zinc antimonide thermoelectric element as a p-type leg of a TE module in transient and steady state

252   under different operating conditions representing practical conditions. To produce more electrical power by using thin

253   film specimen, the heat flow runs laterally in the thermoelectric element. The Transient Seebeck coefficient is

254   introduced in details to analyze behavior of the thermoelectric element. The results show that the Seebeck coefficient in

255   steady state condition increased to a maximum value (242 µV/K) and then reduces as the hot side temperature increases.

256   The bipolar transport is the main reason of reducing the Seebeck coefficients from hot side temperature 275 °C to 350

257   °C. It is shown that the bipolar transport effect is a localized phenomenon. This study considered stability behavior

258   tracking of the thermoelectric element operating under different load conditions at wide range of temperature. The

259   obtained load resistance corresponding to peak power output is shown to be a function of temperature. Also, by

260   increasing the hot side temperature, the maximum output power, figure of merit, and the efficiency of the specimen is

261   enhanced. The thin film specimen showed that can operate in relatively high range of temperature with long operation

262   period without failure or degradation in its thermoelectrically performance.

263

268

269   **References**

270   [1] G.J. Snyder, E.S. Toberer, Nat. Mater. 105, 7 (2008).

271   [2] C.J. Vineis, A. Shakouri, A. Majumdar, M.G. Kanatzidis, Adv. Mater. 3970, 22 (2010).

272   [3] Z.H. Zheng, P. Fan, P.J. Liu, J.T. Luo, X.M. Cai, G.X. Liang, D.P. Zhang, F. Ye, Y.Z. Li, Q.Y. Lin, Appl. Surf. Sci.

273   823, 292 (2014).

274   [4] H. Ohta, S.W. Kim, Y. Mune, T. Mizoguchi, K. Nomura, S. Ohta, T. Nomura, Y. Nakanishi, Y. Ikuhara, M. Hirano,

275   H. Hosono, K. Koumoto, Nat. Mater. 129, 6 (2007)

276   [5] Z.H. Zheng, P. Fan, J.T. Luo, P.J. Liu, X.M. Cai, G.X. Liang, D.P. Zhang, Y. Fan, Intermetallics. 18, 64 (2015).

277   [6] E. Hatzikraniotis, K.T. Zorbas, I. Samaras, T.H. Kyratsi, K.M. Paraskevopoulos, J. Electron. Mater. 2112, 39

278   (2010).

279   [7] Y. Sun, M. Christensen, S. Johnsen, N.V. Nong, Y. Ma, M. Sillassen, E. Zhang, A.E.C. Palmqvist, J. Bøttiger, B.B.

280   Iversen, Adv. Mater. 1693, 24 (2012).

281   [8] Y. Yan, J.A. Malen, Energy Environ. Sci. 1267, 6 (2013).

282   [9] P. Fan, W.F. Fan, Z.H. Zheng, Y. Zhang, J.T. Luo, G.X. Liang, D.P. Zhang, J. Mater. Sci: Mater. Electron. 5060, 25

283   (2014).

284   [10] P. Fan, Z.H. Zheng, Y.Z. Li, Q.Y. Lin, J.T. Luo, G.X. Liang, X.M. Cai, D. Zhang, F. Ye, Appl. Phys. Lett. 106

285   (2015).

286   [11] P. Brinks, N.V. Nong, N. Pryds, G. Rijnders, M. Huijben, Appl. Phys. Lett. 143903, 106 (2015).

287   [12] M.V. Daniel, M. Friedemann, J. Franke, M. Albrecht, Thin Solid Films. 203, 589 (2015).

288   [13] H.C. Shim, C.S. Woo, S. Han, ACS Appl. Mater. Interfaces. 17866, 7 (2015).

289   [14] P. Fan, Z.H. Zheng, Z.K. Cai, T.B. Chen, P.J. Liu, X.M. Cai, D.P. Zhang, G.X. Liang, J.T. Luo, Appl. Phys. Lett.

290   033904, 102 (2013).

291   [15] H. Yin, A.B. Blichfeld, M. Christensen, B.B. Iversen, ACS Appl. Mater. Interfaces. 10542, 6 (2014)

292   [16] D.B. Xiong, N.L. Okamoto, H. Inui, Scripta Materialia. 397, 69 (2013).

293

294

295

296

297

298

299

300

301

302

303

304

11

Figures

310
311
312
313
314
315
316
317
318
319
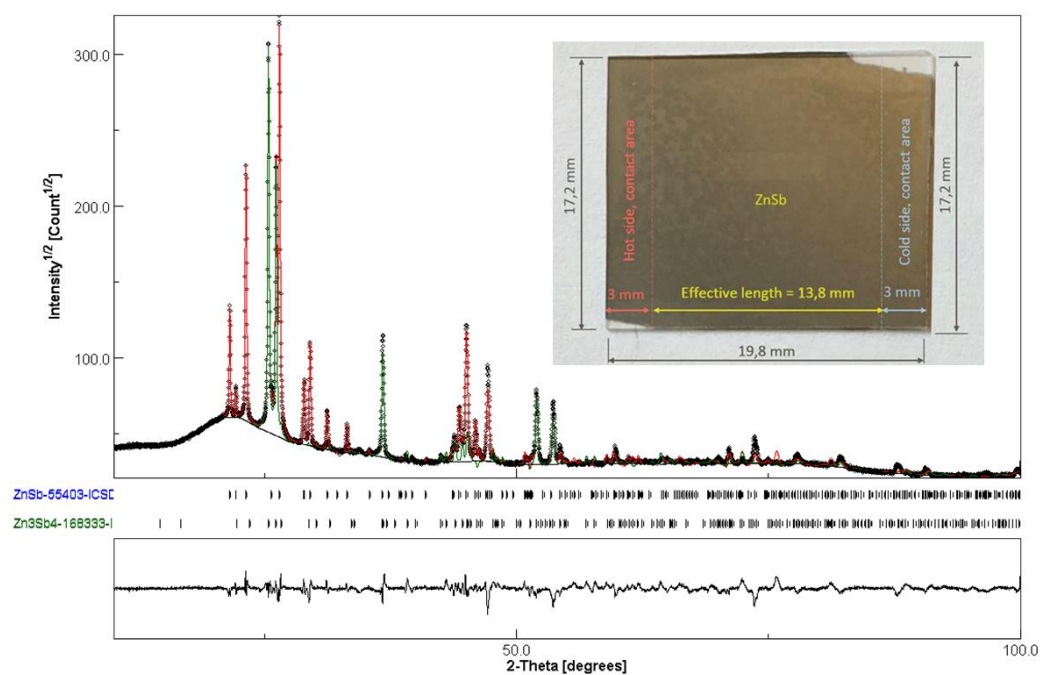
Fig.1: XRD patterns of Zn-Sb thin film and geometric parameters of the specimen

321
322
323
324
325
326
327
328
329
330

331
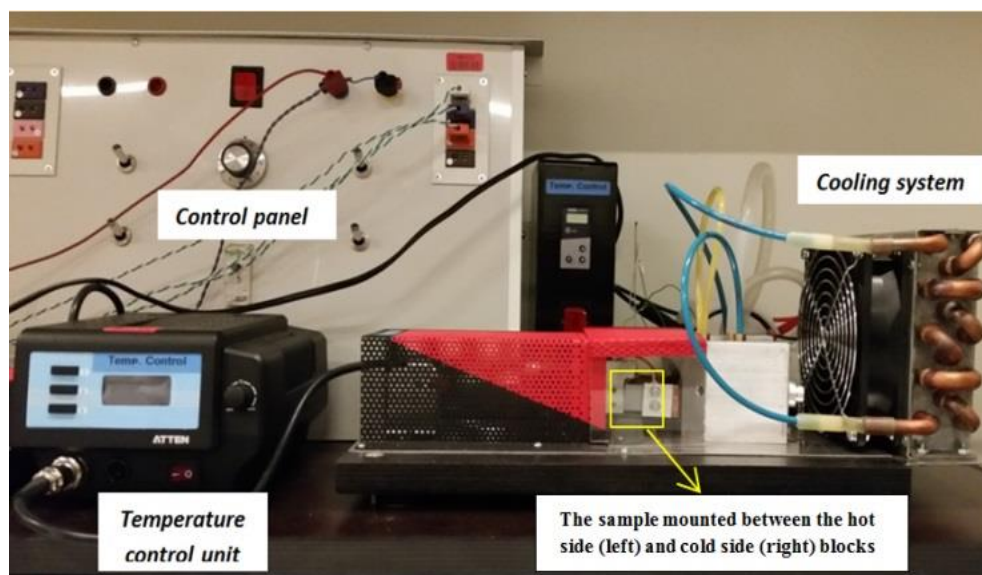
332   **Fig.2: Experimental apparatus**

333

334

335

336

337
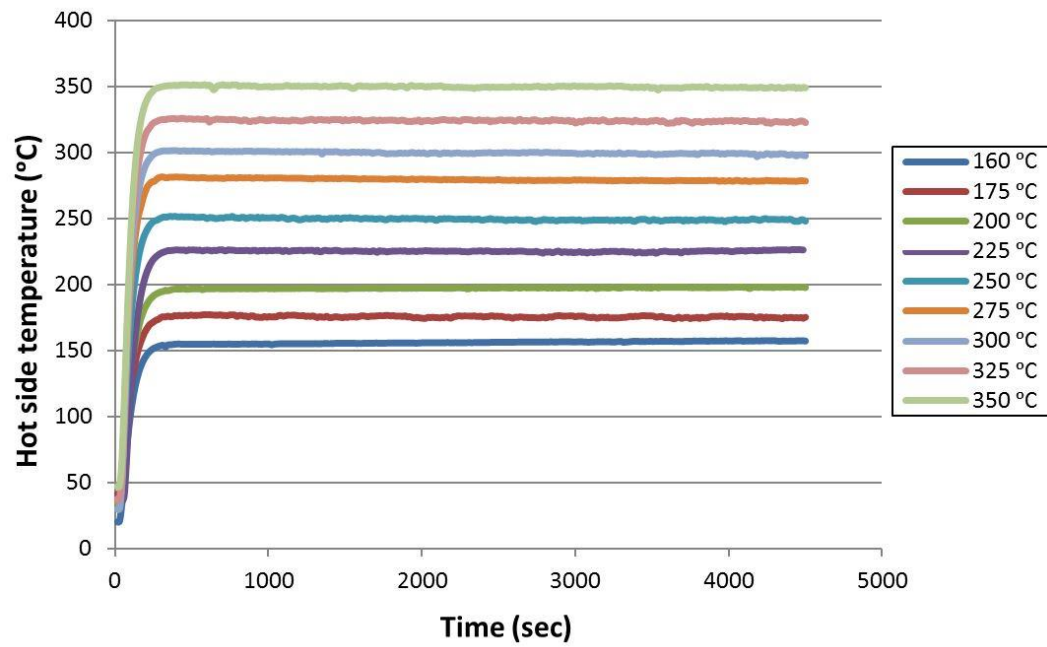
Fig.3: Hot side temperature versus time

339

340
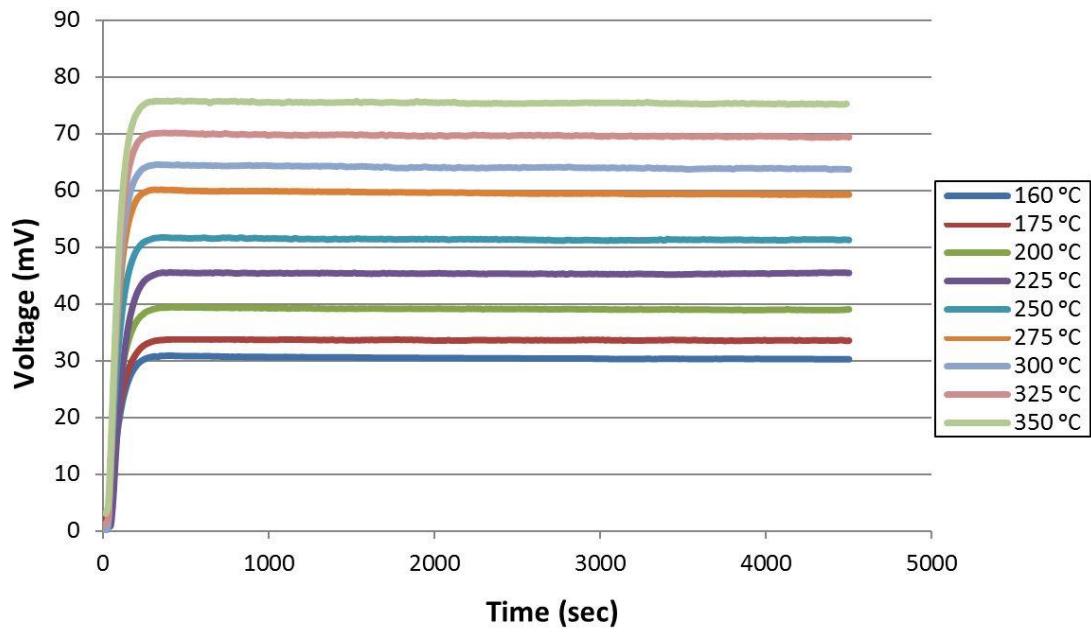
341   **Fig.4: Voltage at different hot side temperatures versus time**

342

343
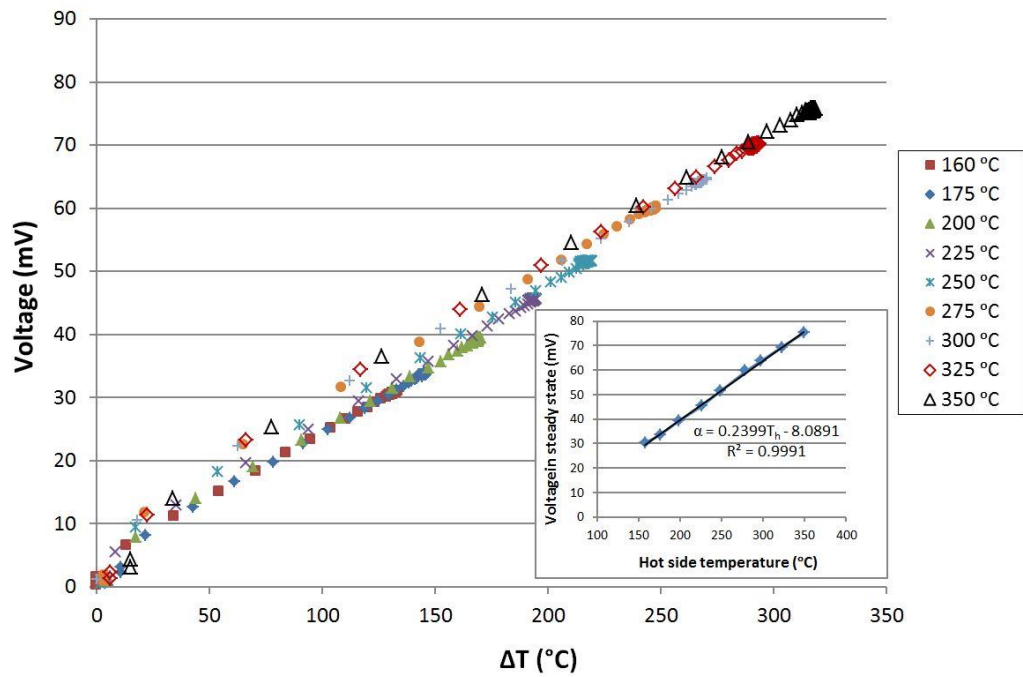
344   **Fig.5: Voltage versus temperature difference, and voltage in steady state versus different hot side temperatures**

345

346
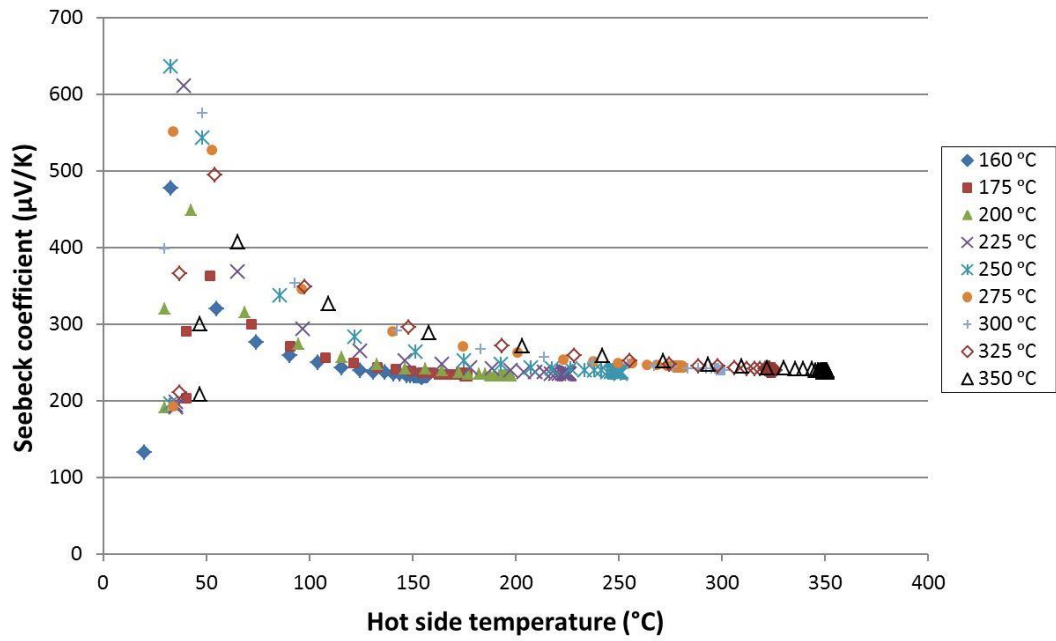
347 **Fig.6: Seebeck coefficient versus hot side temperature**

348

349

350
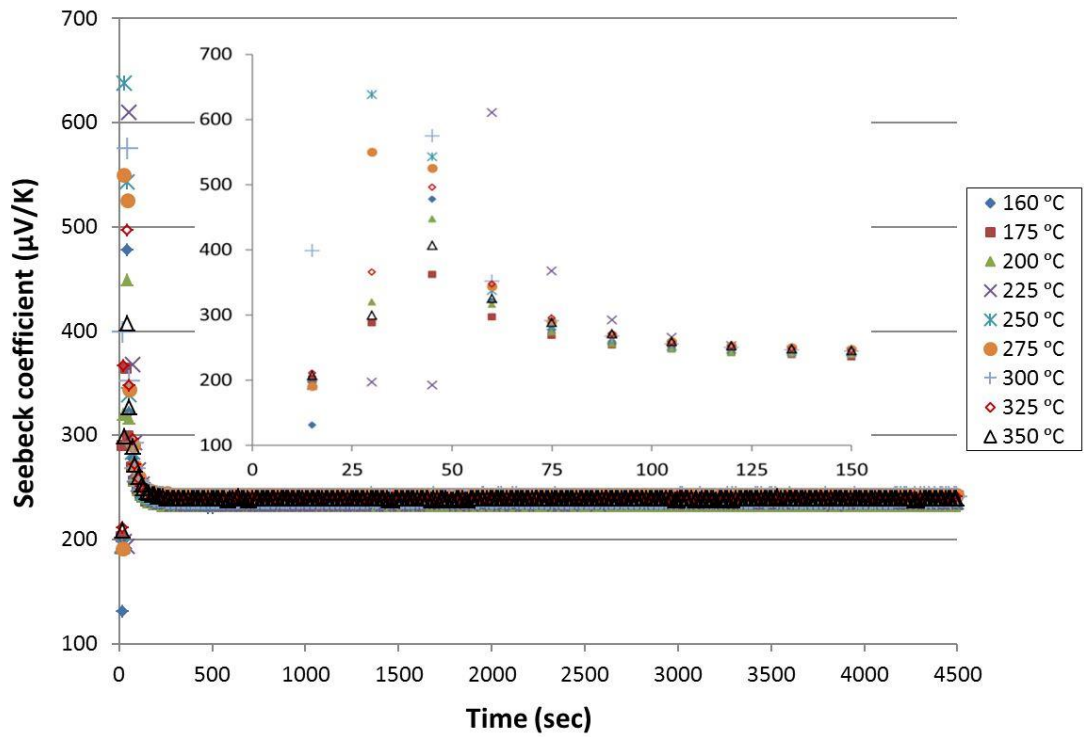
351 **Fig.7: Seebeck coefficient versus time**

15

352

353
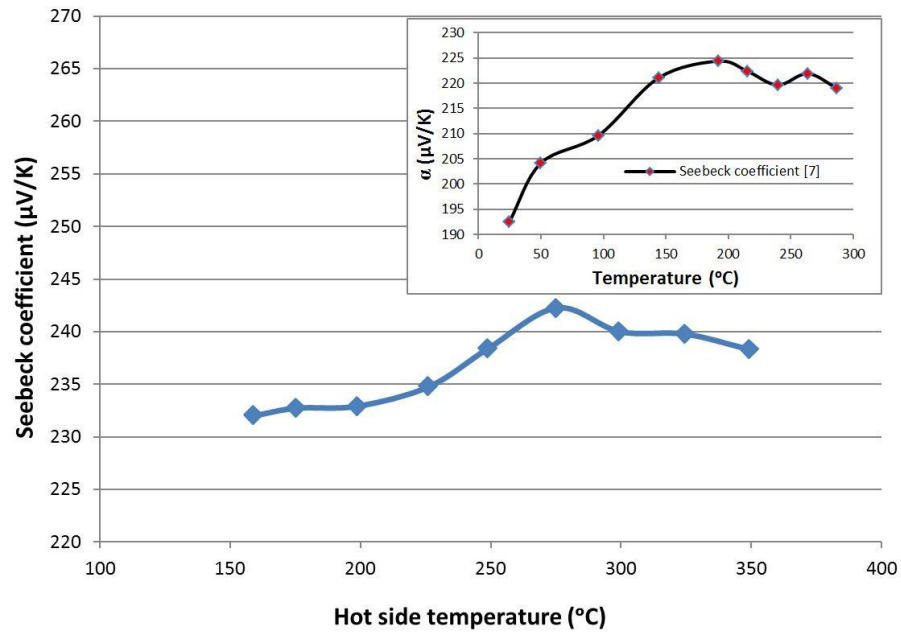
Fig.8: Seebeck coefficient in steady state versus hot side temperature of the specimen

356

357

358

359

360

361

362

363

364

365

366

367

368

369
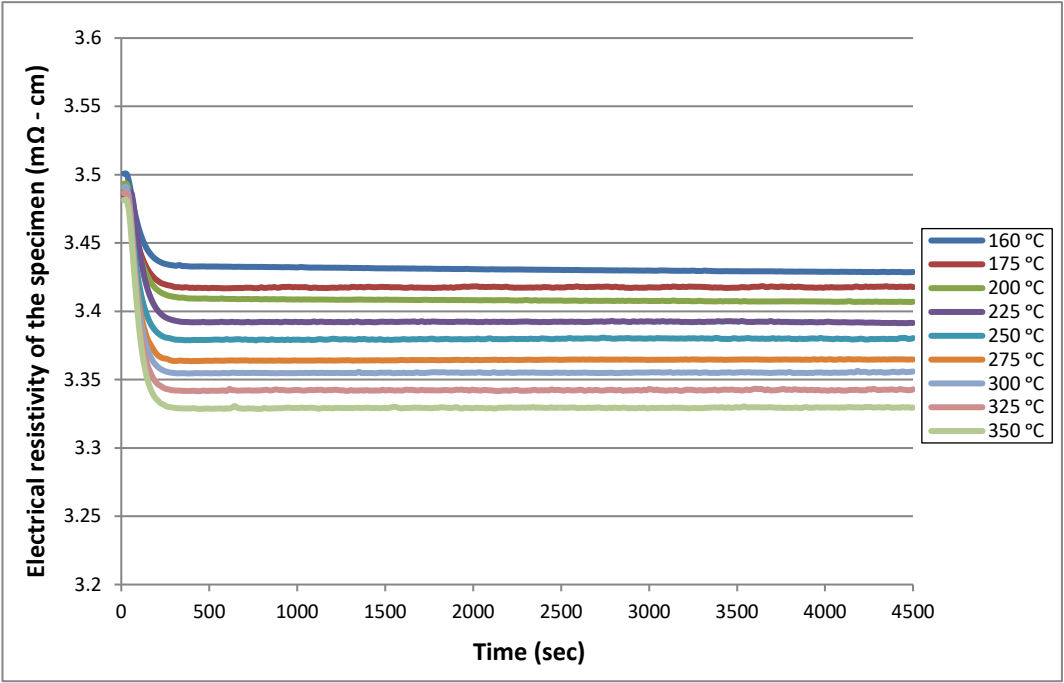
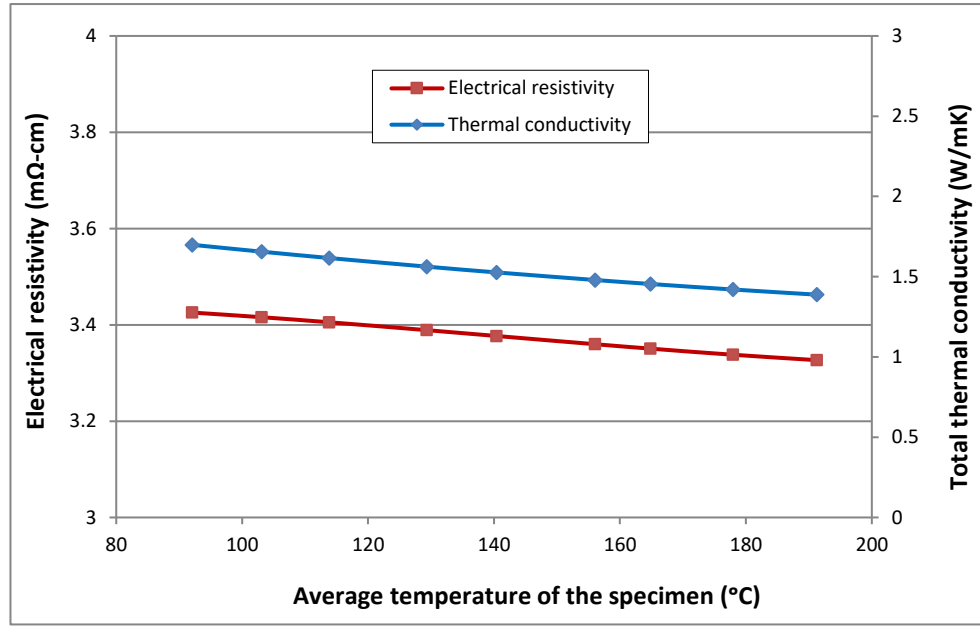**Fig.9: Electrical resistivity of the specimen versus time**

Fig. 10: Electrical resistivity and thermal conductivity in steady state versus average temperature of the specimen
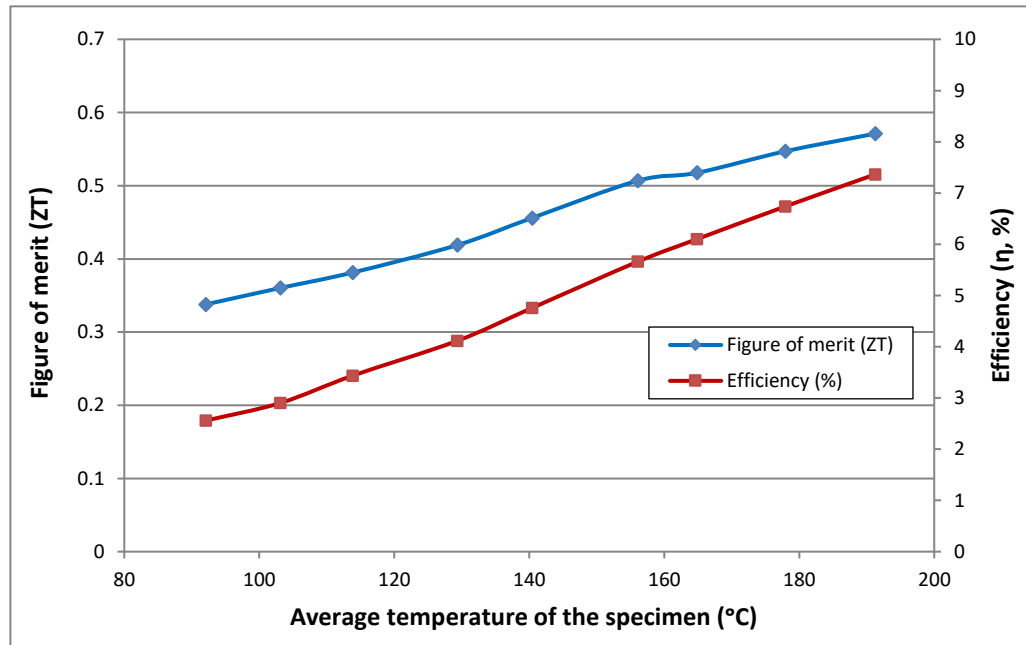

Fig. 11: Figure of merit and efficiency of the thermoelectric element versus average temperature

398
399
400
401
402
403
404
405
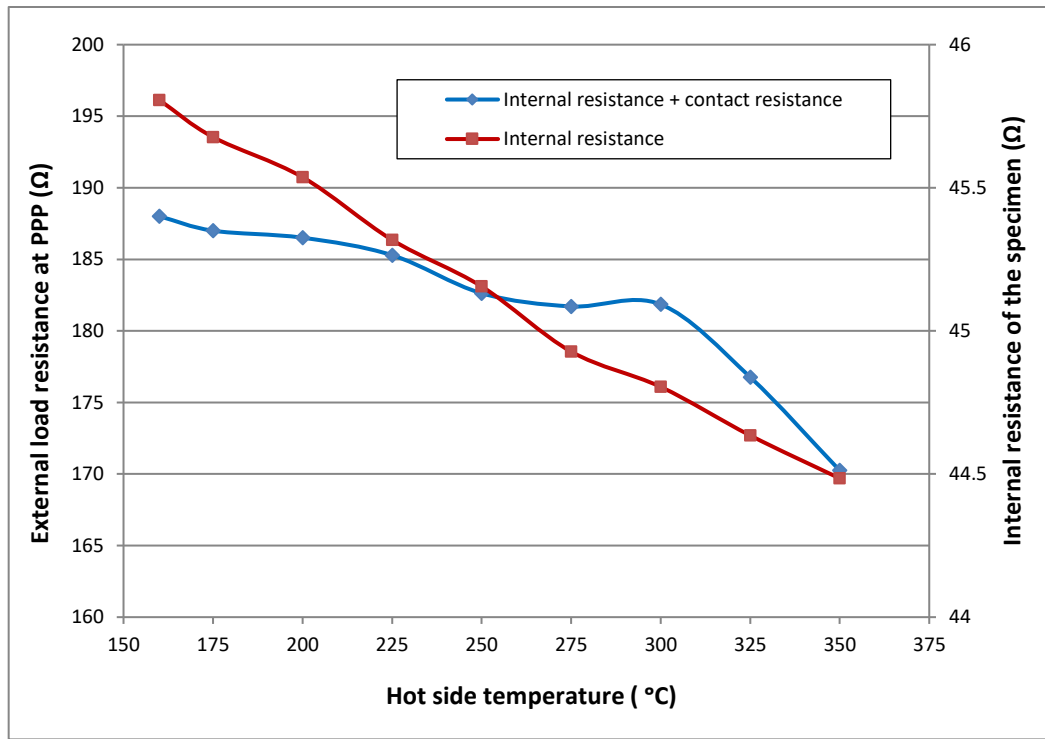406
407
408
409
410
411
412
413
414
415

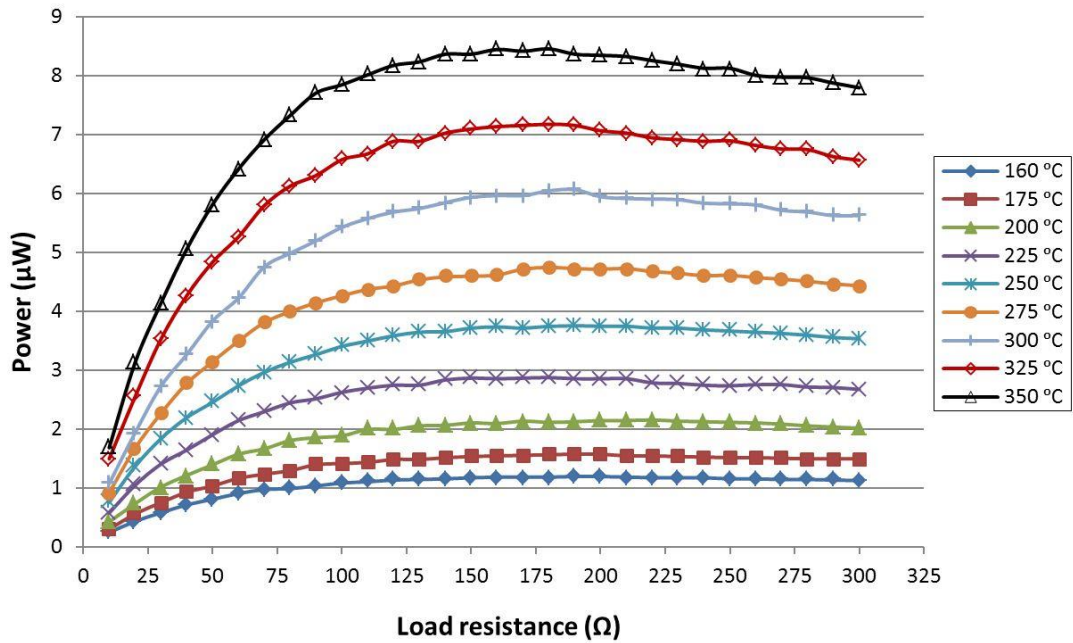**Fig. 12: Electrical resistance with /without considering contact resistance**

Fig.13: Output power by considering contact resistance versus applied load resistances
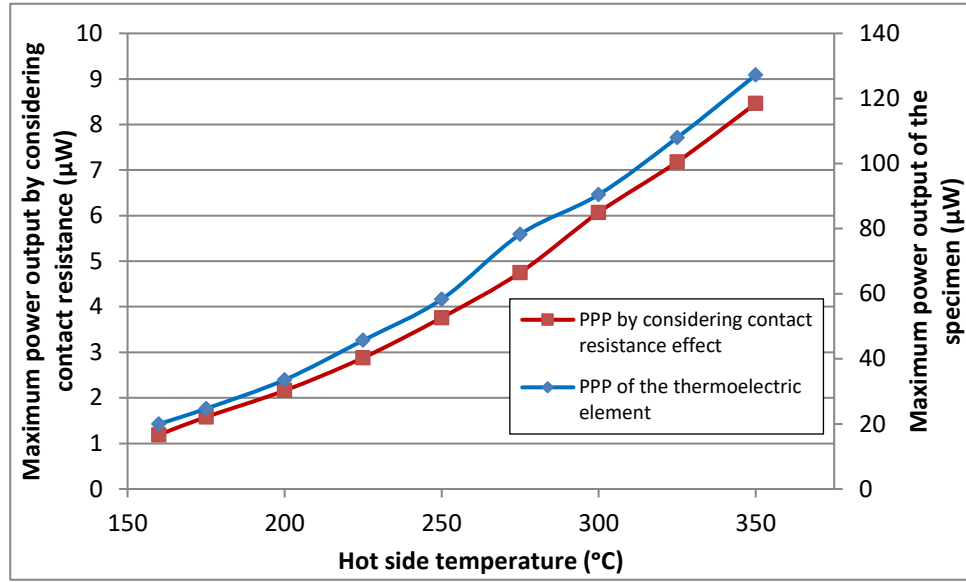
416

417

418

Fig. 14: Maximum power output with/without considering contact resistance effect

429

430

431

Tables

433

434

Table 1: Composition of the film determined by EDX

at% (Zn)	σ (at% (Zn))	at% (Sb)	σ (at% (Sb))
57.6	1.8	42.4	1.3

436